Optical Coherence Tomography: History, Current Status, and Laboratory Work

Michelle L. Gabriele,[1,2,3] *Gadi Wollstein,*[1] *Hiroshi Ishikawa,*[1,2] *Larry Kagemann,*[1,2] *Juan Xu,*[1] *Lindsey S. Folio,*[1] *and Joel S. Schuman*[1,2,3,4]

Optical coherence tomography (OCT) imaging has become widespread in ophthalmology over the past 15 years, because of its ability to visualize ocular structures at high resolution. This article reviews the history of OCT imaging of the eye, its current status, and the laboratory work that is driving the future of the technology. (*Invest Ophthalmol Vis Sci.* 2011;52: 2425–2436) DOI:10.1167/iovs.10-6312

Optical coherence tomography (OCT) has advanced considerably since it was first applied to the eye.[1–7] It is an extension of a technique called low-coherence interferometry, which was initially applied to ophthalmology for in vivo measurements of eye axial length.[1] At the time of introduction, it was used to obtain in vivo optical cross sections of the anterior segment,[6] as well as retinal diseases, such as macular detachment, macular hole, epiretinal membrane, macular edema, and idiopathic central serous chorioretinopathy.[4] OCT cross sections were also used to evaluate the optic disc and retinal layers[5,8] such as the retinal nerve fiber layer (RNFL).[9] Scan patterns that enabled reproducible measurements were developed,[10] and these eventually became incorporated into a commercial system, which had an axial resolution of ~10 μm.

The first clinical system was limited to a scanning speed of 400 axial scans (A-scans)/s because of a physical constraint: a moving reference mirror. OCT uses low coherence interferometry to obtain A-scan intensity profiles, and the process requires light to be split and sent to both a reference arm with a mirror and to the sample. Provided the path length to the reference mirror and tissue match to within the coherence length of the light source, when the reflected beams recombine, interference occurs. Intensity information, in the form of a reflectivity profile in depth, can be extracted from the interference profile. Changing the location of the reference mirror allows backscattered tissue intensity levels to be detected from different depths in the tissue sample. This approach is referred to as time-domain (TD)-OCT because time-encoded signals are obtained directly. Several improvements in OCT hardware have been introduced since the first commercial TD-OCT system became available. Better axial resolution[11–13] and increased scanning speed[14–23] are the two main advancements that have recently become incorporated into commercial systems.

The implementation of broadband light sources into OCT systems[11] improved the axial resolution from ~10 μm to as high as 2 μm in tissue.[24] Acquisition speed has improved considerably by detecting backscattering signals in the frequency domain,[14–23] which means backscattered depth information at a given location can be collected without the movement of a reference mirror. Frequency information is acquired with a broad-bandwidth light source, charge-coupled device (CCD) camera, and a spectrometer[14,17,18,20] or by sweeping a narrow-bandwidth source through a broad range of frequencies with a photodetector.[16,21–23] The approach that incorporates a broadband light source is often referred to as spectral-domain (SD)-OCT, whereas the latter is termed swept-source (SS)-OCT. In both approaches, intensity profiles (A-scans) are obtained using a Fourier-transform of the detected frequencies, and this facilitates rapid A-scan collection. In addition to improved scanning speed, frequency-domain-OCT also offers the advantage of higher detection sensitivity—that is, it exhibits higher signal-to-noise, given a perfect reflector.[23,25] A summary of OCT detection techniques can be seen in Table 1.

With these speed and sensitivity improvements, it is now feasible to collect volumetric (three-dimensional; 3D) scans of tissue, whereas in the past, the amount of time required to do this would have been prohibitive. Broadband volumetric retinal imaging with SD-OCT at speeds of up to 312,500 A-scans/s[26] and SS-OCT at 249,000 A-scans/s[27] have been demonstrated. To date, most clinical systems operate at an acquisition rate of ~27,000 A-scans/s and an axial resolution of 5 to 6 μm. A summary of the current commercially available retinal imaging systems is presented in Table 2.

Current Status of OCT in the Clinic

Glaucoma

Conventionally, the most common scan patterns in TD-OCT glaucoma imaging were a 3.4 mm scan around the optic nerve head (ONH) and six equally spaced radial scans through the macula (6 mm) and optic nerve (4 mm). RNFL thickness is obtained via automated RNFL segmentation in the circumpapillary scan protocol, whereas macular thickness (internal limiting membrane [ILM] to the photoreceptor inner segment-outer [IS–OS] segment junction) is automatically segmented in the macular scan pattern. The optic nerve scan is used to obtain cup area, disc area, cup diameter, disc diameter, and rim area.

From the [1]Department of Ophthalmology, UPMC Eye Center, Eye and Ear Institute, Ophthalmology and Visual Science Research Center, University of Pittsburgh School of Medicine, Pittsburgh, Pennsylvania; the [2]Department of Bioengineering, Swanson School of Engineering and the [4]McGowan Institute for Regenerative Medicine, University of Pittsburgh, Pittsburgh, Pennsylvania; and the [3]Center for the Neural Basis of Cognition, University of Pittsburgh and Carnegie Mellon University, Pittsburgh, Pennsylvania.

Supported in part by National Institutes of Health Grants R01-EY13178 and P30-EY08098; The Eye and Ear Foundation, Pittsburgh, PA; and an unrestricted grant from Research to Prevent Blindness, New York, NY.

Submitted for publication July 30, 2010; revised October 20, 2010; accepted November 13, 2010.

Disclosure: **M.L. Gabriele**, None; **G. Wollstein**, Carl Zeiss Meditec (F), Optovue (F), P; **H. Ishikawa**, P; **P.L. Kagemann**, None; **J. Xu**, P; **L.S. Folio**, None; **J.S. Schuman**, Carl Zeiss Meditec (F), P

Corresponding author: Joel S. Schuman, UPMC Eye Center, Department of Ophthalmology, University of Pittsburgh School of Medicine, 203 Lothrop Street, Eye and Ear Institute, Suite 816, Pittsburgh, PA 15213; schumanjs@upmc.edu.

TABLE 1. Comparison of TD-, SD-, and SS-OCT Devices

	Light Source	Ophthalmic System Commercially Available?	Primary Advantages	Primary Disadvantages
TD-OCT	Broadband width	Yes	Intensity information acquired in time domain; no complex conjugate image	Moving reference mirror required limiting acquisition rate
SD-OCT	Broadband width	Yes	No moving reference mirror required; higher sensitivity than TD-OCT; high scanning speed and axial resolution have been attained	Noticeable signal drop-off with depth
SS-OCT	Narrow band, swept through broad range	No	No moving reference mirror required; Higher sensitivity than TD-OCT; very high scanning speeds can be attained; minimal signal drop-off with depth	Most ophthalmic systems operating at longer wavel engths ($\lambda = 1-1.3$ μm), with lower axial resolution

These ONH parameters are obtained automatically: the software detects the ONH margin/RPE tips, but the user can modify the location if the ONH margin detection algorithm is inaccurate.

The ONH and RNFL scan protocols have been used since TD-OCT became commercially available, and RNFL and ONH parameters have been shown to differ between glaucomatous and healthy eyes.[9,28–33] The glaucoma-discriminating ability, measured by the area under receiver operating characteristic curves (AROC) of RNFL (AROC = 0.94) and disc parameters (e.g., rim area AROC = 0.97), has been reported to be higher than macular volume and thickness (AROC, both 0.80).[34] A similar glaucoma-discriminating ability is seen in comparing TD-OCT imaging and SD-OCT imaging when similar parameters are examined.[35] However, it may be possible to further improve glaucoma discrimination using parameters obtained from 3D scanning. With the commercialization of rapidly scanning SD-OCT systems, 3D volumes of tissue are now easily acquired. A 3D dataset not only allows a quantitative analysis from more locations but, once a volume has been collected, OCT fundus (en face) images can be obtained by integrating A-scans.[20] These can be used for a subjective assessment of signal quality and to assist with evaluating and/or correcting eye motion that may have occurred throughout the scan. The OCT fundus image also allows registration of OCT cross sections to precise retinal locations.

Acquisition of 3D datasets has led to the advancement of software methods for efficiently analyzing and summarizing these vast amounts of data. One method of obtaining RNFL thickness measurements has been sampling the 3D volume (e.g., $6.0 \times 6.0 \times 2.0$ mm, centered on the ONH) after acquisition, at a diameter of 3.4 mm centered on the ONH (Fig. 1). This method has been shown to have higher reproducibility than the conventional TD-OCT 3.4 mm scan circle, where the image is acquired along the circle only.[36] One explanation for the improved performance is that, with TD-OCT, scan placement is dependent on the user and can be variable, but with SD-OCT, the circle can be consistently placed in the same location by using landmarks within the 3D volume.

Although sampling 3D volumes after acquisition may be an effective way of summarizing RNFL measurements, it is doing so at a cost: data outside the 3.4-mm band are not being used. Subjectively, wedge defects and global thinning may be easy to spot, but subtle changes or deviations from normal outside the 3.4-mm sampling band may be missed. One way of addressing this is to create an RNFL thickness map, which consists of all thickness measurements outside of the ONH. From this, thickness measurements from one subject can be compared to population thickness measurements. To date, however, commercial software is available for looking at deviation from normal, but there is no quantitative assessment using all available RNFL information.

Different approaches have been proposed for quantifying 3D data. 3D RNFL thickness has been analyzed in terms of a thickness profile as distance from the ONH increased.[37] In healthy eyes, the slope of RNFL thickness increases near the margin of the ONH, peaks, and then decreases with increasing distance from the ONH center in all but the nasal quadrant, which linearly decreases starting from the disc margin. An-

TABLE 2. Description of Commercially Available SD-OCT Systems

Device (Manufacturer)	Description
3D-OCT 2000 (Topcon, Tokyo, Japan)	SD-OCT and high-resolution fundus camera; axial resolution, 5 μm; A-scan acquisition rate, 27 kHz.
Bioptigen SD-OCT (Bioptigen, Research Triangle Park, NC)	Designed for both clinical and research use and includes a hand-held probe and microscope setup; axial resolution, 4 μm; A-scan acquisition rate, 20 kHz
Cirrus HD-OCT (Carl Zeiss Meditec, Dublin, CA)	Software includes guided progression analysis for glaucoma progression detection; axial resolution, 5 μm; A-scan acquisition rate, 27 kHz.
RTVue-100 (Optovue, Fremont, CA)	Offers multiple scanning protocols for glaucoma detection, including ganglion cell complex analysis; axial resolution, 5 μm; A-scan acquisition rate, 26 kHz.
SOCT Copernicus (Optopol, Zawiercie, Poland)	Software includes progression analysis software that incorporates disk damage likelihood scale, asymmetry between the discs, and RNFL thickness; axial resolution, 6 μm; A-scan acquisition rate, 27 kHz.
Spectral OCT SLO (Opko, Miami, FL)	Combines SD-OCT, scanning laser ophthalmoscopy, and microperimetry. Axial resolution, 6 μm, A-scan acquisition rate, 27 kHz.
Spectralis OCT (Heidelberg Engineering, Heidelberg, Germany)	High-speed SD-OCT device with eye-tracking, fluorescein angiography, ICG angiography, and autofluorescence. Axial resolution, 4 μm; A-scan acquisition rate, 40 kHz.

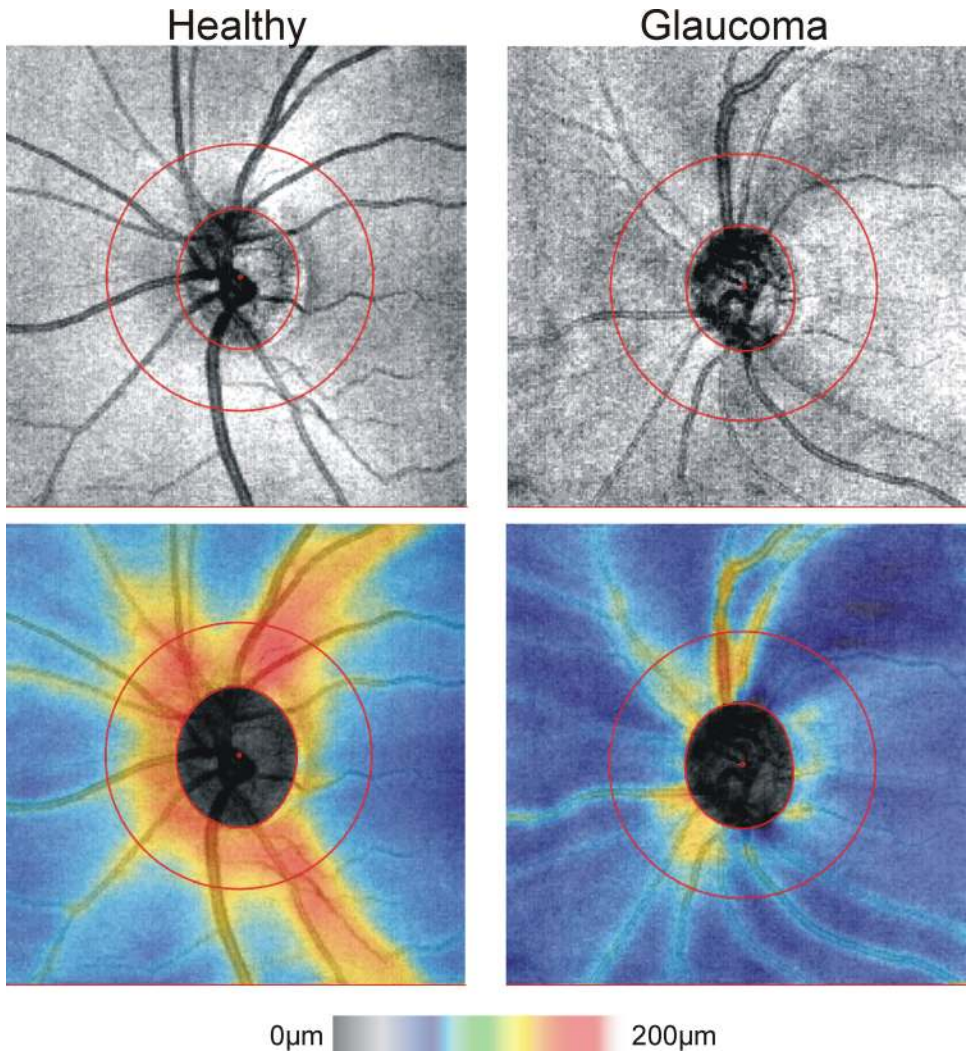

FIGURE 1. *Top*: OCT fundus images; *bottom*: RNFL thickness maps obtained by segmenting RNFL at all locations outside of the optic nerve, for a healthy and glaucoma subject. *Outer red circle*: the location of a resampled 3.4-mm peripapillary cross-section. Images acquired with Cirrus HD-OCT; 200 × 200 A-scans, 6 × 6 mm.

other approach (Ishikawa H et al. *IOVS* 2009;50:ARVO E-Abstract 3328) exploits 3D macular data, which have been summarized using segmentation of the inner retinal complex (IRC: retinal ganglion cell layer [RGC], inner plexiform layer [IPL], inner nuclear layer [INL]; Fig. 2).[38] This approach reduces IRC data to superpixels (4 × 4 adjacent sampling points) and compares these superpixels to a normative thickness superpixel dataset. By condensing measurements into superpixels, it is less likely that small imaging artifacts or algorithm failure will have an effect.

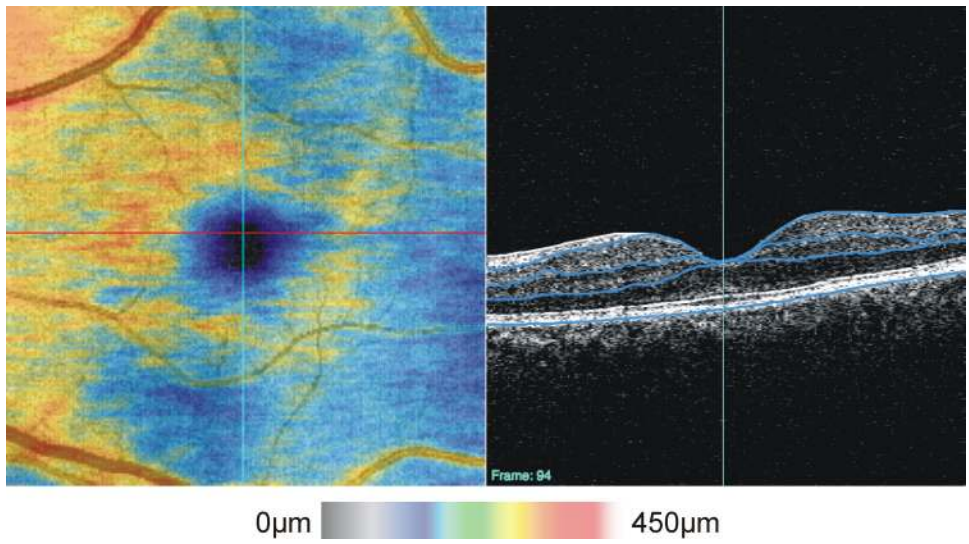

FIGURE 2. *Left*: SD-OCT macular thickness map (inner retinal complex); *right*: cross-sectional image showing automated segmentation results for one frame of the 3D volume. Image acquired with Cirrus HD-OCT; 200 × 200 A-scans, 6 × 6 mm); *Blue lines*: from inner to outer retina, indicate the outer border of the retinal nerve fiber layer, outer border of the inner plexiform layer, outer border of the outer plexiform layer and RPE.

One commercially available system has developed an approach for summarizing macular data called the Ganglion Cell Complex (GCC; RTVue, Optovue, Inc) which consists of essentially the same layers as the IRC: the RGC (retinal ganglion cell bodies), RNFL (RGC axons) and IPL (RGC dendrites). The GCC measurements are then directly compared to a normative database and thickness difference and significance maps are available (Fig. 3).

While a comparison to a normal population may reveal differences, structural changes may be occurring while a patient remains within normal limits and therefore go undetected. Ideally, a longitudinal comparison could be made for a given individual to look for subtle structural changes attributed to disease progression. One approach, proposed by Kim et al.,[39] is to allow compatibility between TD-OCT and 3D OCT device iterations. Since TD-OCT devices have been commercially available longer than 3D imaging systems, years of patient information may be available. The method presented by Kim et al. resamples a 3D-OCT dataset for every possible 3.4-mm circular scan location within the boundaries of the 3D-OCT volume. It then uses cross correlation between these virtual circular scans and the TD-OCT 3.4-mm scan to automatically match the TD-OCT scan circle location within the volume.

To longitudinally compare 3D volumes, however, image registration techniques must be developed to spatially align 3D scans before they can be compared. This may be accomplished using cross-correlation,[40,41] or by using landmarks within the OCT fundus image, such as blood vessels.[42,43] Eye motion during acquisition has been shown to alter scan location,[44–46] and the effect of eye motion is visible on OCT en face images as discontinuous blood vessels. Detecting and correcting blood vessel location to align the OCT fundus can help correct eye motion,[42] which may be useful for cross-sectional analysis.

Longer wavelength imaging (~1-μm center wavelength) of the lamina cribrosa[27] and birefringence imaging of the RNFL using polarization-sensitive (PS)-OCT[47–49] are two techniques under development that may improve the diagnosis and monitoring of glaucoma. These are further described in the Preclinical and Laboratory Studies section of this review.

Retina

The macular scan pattern discussed above—six radial macular scans, 6 mm long, spaced 30° apart—has traditionally been used in TD-OCT imaging to assess retinal parameters such as total retinal thickness and the IRC. Three-dimensional imaging; however, has revolutionized the examination of retinal disease.[50–55] An examination of the 3D structure of the retina, as opposed to just six radial scans, may make subtle structural changes apparent. For example, using high-resolution 3D imaging to observe the photoreceptor IS–OS junctions may be an indicator of visual outcomes after macular hole surgery.[56–58]

At present, one application of 3D OCT of imaging retinal diseases that has considerable clinical potential is surgical planning and the evaluation of surgical outcomes. The use of OCT for planning an access point to release the hyaloid for vitrectomy using the six radial scan pattern in TD-OCT has been described.[59] Although this was effective for minimizing traction forces on the macula during surgery, a detailed 3D map of the hyaloid membrane and subhyaloid space could further inform the clinician. Falker-Radler et al.[60] used 3D imaging to visualize the vitreomacular interface in subjects who were undergoing surgery for epiretinal membrane. Others have used OCT for evaluation of structure after surgery for macular hole[57,58,61] and vitreomacular traction.[52,62–64] The use of 3D imaging for surgical preparation and evaluation of surgical outcomes has the potential to improve with the use of longer wavelength imaging, which is described later in this review. Automated segmentation of structures of interest, when possible, may provide objective measurements to clinicians for pre- and postsurgical evaluation.

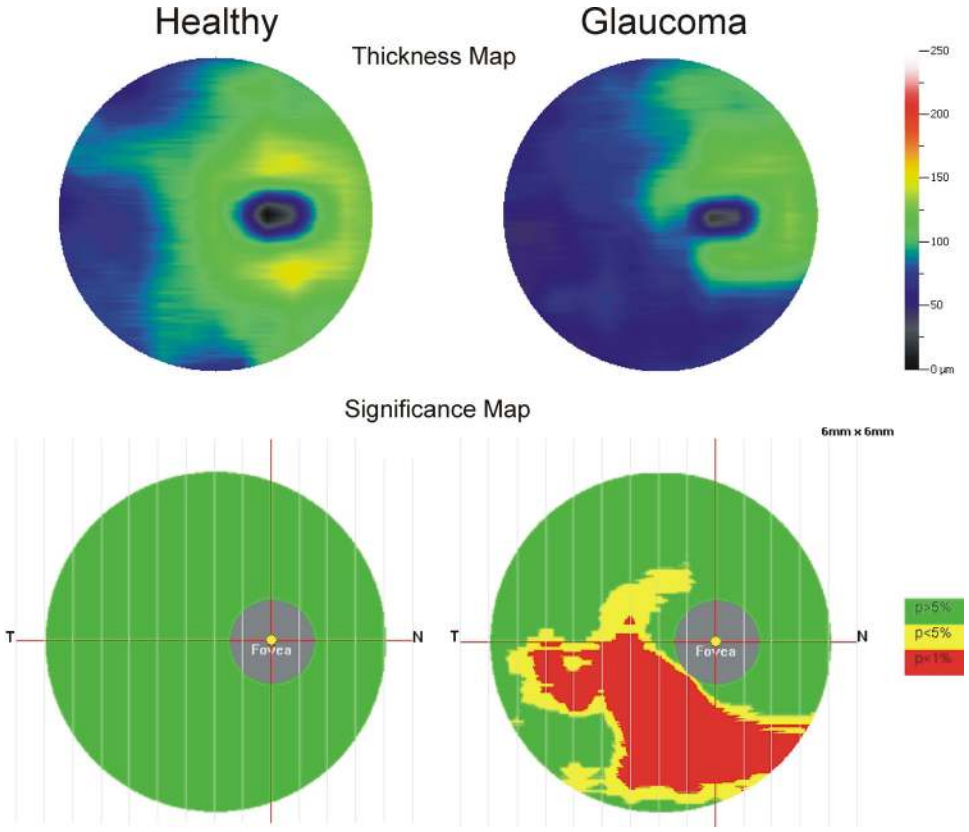

Figure 3. Ganglion cell complex thickness and significance maps for a healthy (*left*) and glaucoma (*right*) subject. The ganglion cell complex includes cell bodies, axons and dendrites of retinal ganglion cells. Images acquired with RTVue-100: 1 horizontal B-scan, and 15 vertical B-scans (separated by 0.5 mm). All B-scans consisted of 933 A-scans; 7 × 6 mm scan area.

Quantification of thickness is possible in certain diseases,[65,66] especially with early stage changes.[67,68] The reproducibility of SD-OCT retinal thickness measurements is higher in than that of TD-OCT.[69] Thickness has been shown to correlate with best corrected visual acuity in diabetic macular edema[70] and ERM.[71] Although thickness may be a clinically useful correlate of visual function, there are cases and diseases in which no correlation to thickness is seen, and thus clinicians should exercise caution in interpretation of thickness measurements.[72]

Drusen volume may be a predictor of progression of age-related macular degeneration,[65] and efforts are under way for automated assessment.[66] Although accurate quantification of volumetric tissue changes will assist with longitudinal monitoring of disease, fully automated segmentation may not be reliable because of shadowing from fluid in the retina[73,74] or because of pathologic events that disrupt normal retinal structures, such as macular hole, subretinal fluid, pigment epithelium detachment, and others.[75,76]

In cases in which fully automated segmentation fails, C-mode visualization of structures may augment subjective analyses.[77] A 3D volume of data can be sectioned in any plane after acquisition, and for C-mode visualization, data are sectioned perpendicular to the retina. The section can be of any thickness, so structures embedded within a volume can be exposed. Often, since the true structure of the retina is curved, exact perpendicular sections slice through several layers simultaneously[78,79]; thus, aligning the volume to structures such as the ILM or RPE assists with isolating structures of interest.[77] Figure 4 shows an example C-mode section taken after aligning a macular SD-OCT 3D volume to the RPE. Moving axially, past the retina and RPE, enables visualization of the choroidal blood vessels. The choroidal vessels are not apparent in the corresponding SD-OCT fundus image because of highly reflective layers superficial to the choroid. The C-mode provides alternative viewing perspective for many retinal diseases, such as cystoid macular edema, central serous retinopathy, vitreoretinal traction, and age-related macular degeneration,[77] and it can improve the visualization of their pathologic features.

It is also possible to image the choroid by focusing the illuminating OCT beam deeper and moving the choroid closer to 0 delay.[80] In addition, longer wavelength imaging at ~1 μm[81] allows for deeper penetration of light into the retina and choroid. A combination of these approaches may improve the current understanding of choroidal diseases.

Correcting ocular aberrations with adaptive-optics (AO)-OCT[82] may also provide a unique viewing perspective for retinal diseases. This technique has been applied to view photoreceptors[83] and RNFL.[84] The utility of longer wavelength imaging and AO-OCT is under investigation and is described in the Preclinical and Laboratory Studies section below.

Anterior Segment

Anterior segment OCT (AS-OCT) provides structural information of the cornea and anterior chamber without contacting the eye, offering an ease of image acquisition and a consider-

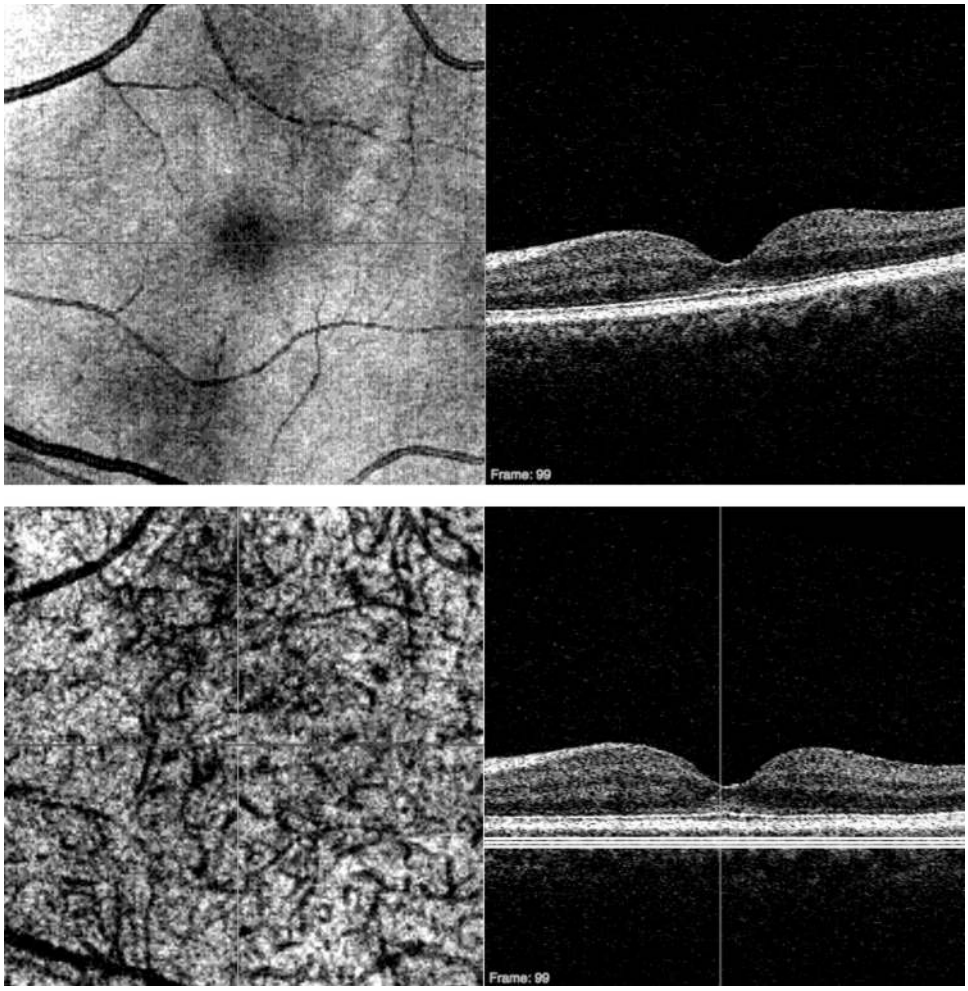

Figure 4. *Top left*: Macular SD-OCT fundus image; *top right:* cross-section through the fovea. *Bottom left*: C-mode of choroidal vessels; *bottom right*: based on a slab of thickness indicated by the *three horizontal white lines* after aligning to the RPE. Image acquired with Cirrus HD-OCT; 200 × 200 A-scans, 6 × 6 mm).

able advantage over ultrasound biomicroscopy (UBM). While it cannot be used to image deep structures such as the ciliary body, as UBM can, AS-OCT has higher axial resolution (5–10 μm for AS-OCT compared with 25 μm for UBM).[85]

It is possible to acquire high-resolution images of the sclera, angle, and iris with AS-OCT imaging at longer wavelengths (1.3 μm).[86] High-resolution images of the anterior chamber angle can also be obtained with 850-nm systems, and this has led to the visualization of the trabecular meshwork and Schlemm's canal.[87–89]

Raster scanning and radial scanning of the cornea have been used to measure thickness,[90] resulting in reliable pachymetric mapping.[91,92] Pachymetric measurements obtained with AS-OCT may assist with planning or follow-up of LASIK patients[93] or may be used to diagnose keratoconus.[94]

In addition to its potential benefits in the evaluation of the anterior chamber angle and cornea, AS-OCT has also been shown to be applicable in the assessment of lens thickness in phakic eyes[95] or intracorneal ring placement.[96] This can provide an alternate, noncontact, method of pre- and postsurgical assessment.

Preclinical and Laboratory Studies

Swept-Source OCT and Longer Wavelength Imaging

As previously discussed, SS-OCT obtains time-encoded spectral information by sweeping a narrow-bandwidth laser through a broad optical spectrum. Backscattered intensity is detected with a photodetector. This process is in contrast to SD-OCT, which uses a broad bandwidth light source and detects the interference spectra with a CCD camera and spectrometer. The use of spectrometer-based SD-OCT has become widespread in the clinic, but there are some benefits to photodetector-based SS-OCT systems. Similar to SD-OCT, SS-OCT offers speed and sensitivity advantages over TD-OCT.[23,27] To date, speeds of up to 249,000A-scans/s have been attained in the eye.[27] Therefore, eye motion artifacts are greatly reduced compared with TD-OCT.[22]

One advantage of SS-OCT over SD-OCT is that it does not require a CCD camera and spectrometer and instead uses a simpler photodetector.[27] A drawback to camera-based SD-OCT detection is a drop-off in signal with depth of scanning because of the finite pixel size of the CCD camera.[25,97] Although this can be improved by reducing the camera pixel size,[97] it increases the complexity and therefore the cost of the CCD array. A noticeable drop-off in signal with depth typically does not occur with SS-OCT imaging due to the narrow bandwidth of the light source.[23,97]

At this time, one disadvantage of SS-OCT is that most systems are now operating at longer wavelengths (λ = 1–1.3 μm), with very few studies demonstrating SS-OCT in the 800 nm range.[98,99] Water absorption limits the usable bandwidth at 1 and 1.3 μm[99] and this limits the axial resolution; the water absorption window at 850 nm is larger, so higher axial resolution can be achieved.

While axial resolution at longer wavelengths may not be as fine as at 850 nm, there are advantages to using ~1- and 1.3-μm sources. Posterior segment imaging using ~1-μm (1040–1060-nm)[81,100,101] center wavelengths has allowed deeper penetration into the retina, optic nerve head, and choroid,[81,102] which may be beneficial for imaging choroidal vessels, lamina cribrosa, and diseases such as choroidal neovascularization.[103] The water absorption window at 1.3 μm offers even deeper penetration of light and may be useful for cornea and anterior segment imaging.[16,22,23,104–106] Anterior chamber imaging at 1310 nm has been applied to visualize anterior segment structures anterior and posterior to the iris, Schlemm's canal, trabecular meshwork, and the scleral spur,[107] as well as the anterior chamber angle.[108]

While SS-OCT systems at any wavelength are not yet commercially available for clinicians, in part due to the cost of the light source, there is clinical potential for such devices. No signal drop-off with depth in SS-OCT, in combination with deeper penetration from longer wavelengths, may improve delineation of the outer retina, RPE, and choroid thereby enhancing the performance of segmentation algorithms. In addition, high-speed 1.3-μm imaging may expand the use of anterior segment OCT imaging.

Adaptive Optics OCT

Ophthalmic systems that employ adaptive optics (AO) dynamically adjust their optical characteristics to compensate for monochromatic aberrations that occur naturally in the eye. AO was initially proposed[109] and later used by astronomers to correct distortions of light passing through the atmosphere.[110] In 1997, AO was demonstrated in the eye by Liang et al.,[111] who used a Hartmann-Shack wavefront sensor and a deformable mirror to correct contrast sensitivity and improve quality of vision for human subjects and to obtain higher resolution images with an AO fundus camera. Shortly thereafter, individual cone mosaics were imaged.[112]

AO-OCT was first reported by Miller et al.[82] in 2003 to improve transverse resolution. Uncorrected, conventional OCT beams 1 mm in diameter have a transverse resolution limited to ~15 to 20 μm.[113] This makes it difficult to visualize individual cellular structures. One way to improve transverse resolution is to increase the numerical aperture, which in practice means increasing the diameter of the OCT beam entering the eye, since this would decrease the spot size on the retina. However, the theoretical diffraction-limited resolution cannot be attained due to ocular aberrations[114] that occur when the pupil is dilated.[115,116] AO-OCT measures and corrects these aberrations using wavefront sensing and deformable mirrors, thereby minimizing spot size and improving transverse resolution. It should also be noted that aberrations can be dependent on the bandwidth of the light source used for OCT imaging,[116] and these may be improved using an achromatizing lens.[117]

Ultrahigh (axial)-resolution AO-OCT was introduced in 2004, improving transverse resolution to 5 to 10 μm in the retina.[113] Zhang et al.[118] developed an AO SD-OCT system and saw an enhancement of the photoreceptor IS–OS junction in vivo with AO. C-mode sectioning of 3D datasets have also facilitated the visualization of axon bundles in the RNFL[84] and cone photoreceptor mosaics from healthy subjects,[83,119] and subjects with structural abnormalities[120] and optic neuropathies.[121]

One disadvantage of AO imaging is that the depth of focus is narrow, which means focusing simultaneously at different depths is difficult. For example, photoreceptors, located deep in the retina, and superficial retinal ganglion cells cannot be brought into focus at the same time. It may be possible to address this limitation by scanning in depth and varying the focal plane[122] or by stitching together volumes.[123] Another limitation to AO imaging is that the field of view is restricted to approximately 1° to 3°; the use of an eye-tracking system to acquire a series of neighboring scans and gradually build up an image covering a larger volume may provide one solution to this limitation.[124]

A potential advantage of improved lateral resolution with AO-OCT is improved understanding of normal and pathologic retinal function in vivo. AO may also help to improve the overall quality of images obtained from eyes that have more

aberrations. Enhanced lateral resolution and improved image quality may then lead to better performance of automated segmentation algorithms and assist with disease diagnosis and follow-up.

Polarization-Sensitive OCT

Polarization-sensitive (PS) OCT detects polarization changes in circularly polarized light.[125] PS-OCT was initially applied to characterize the birefringence of tooth enamel,[126] skin,[127] and cartilage.[128] In 2001, PS-OCT was first used in the eye[129] to measure birefringence of the RNFL in rhesus monkeys. RNFL birefringence was measured in humans by Cense et al.[47,48] and Yamanari et al.,[49] who found that, unlike RNFL thickness, birefringence does not change as a function of increasing radius from the ONH.[48] It does, however, vary by sector around the ONH, with higher birefringence in thicker areas.[48] Because birefringence may change with disease, RNFL birefringence obtained with OCT may eventually provide an additional indicator of glaucomatous change. The utility of PS-OCT in glaucoma detection and monitoring is currently under investigation. In addition to measuring RNFL birefringence, a longer wavelength ($\lambda = 1.3$ μm) PS-OCT system has been used to observe the anterior chamber in subjects after glaucoma surgery.[108] A swept-source PS-OCT system at a 1-μm center wavelength was used to image sclera and lamina cribrosa,[130] which may provide insight into structural changes occurring in the ONH in glaucoma.

Polarization of the RPE may be important in the detection of macular disease.[131,132] Gotzinger et al.[132] developed a segmentation algorithm based on what they refer to as the "polarization scrambling effect " of the RPE, which provides an alternative to conventional intensity-based quantification. A combined AO PS-OCT system was later used to measure RPE polarization scrambling.[133] Conventional PS-OCT was used to observe subjects with AMD,[134,135] where abnormal birefringence was colocalized with exudative lesions.

PS-OCT has been used for anterior segment imaging to measure corneal birefringence,[136,137] and these measurements were used to compensate for corneal birefringence in retinal imaging.[138] A difference in polarization in healthy corneas versus those with keratoconus was demonstrated in vitro, suggesting that PS-OCT may eventually provide insight into corneal diseases in vivo.[139]

The aforementioned studies indicate that PS-OCT offers an alternative approach for detecting changes of optical properties in tissue. If it can be established that a change in birefringence occurs before tissue thinning or thickening, it may allow earlier detection and the opportunity for earlier intervention.

Eye-Tracking OCT Systems

Subject eye motion can alter the intended location of an OCT scan. Attempts to correct eye motion by using postprocessing methods are under development, but real-time eye-tracking systems may provide an alternate method of avoiding eye motion artifacts.[46] Menke et al.[140] showed that an SD-OCT system with built-in eye-tracking can provide reproducible measurements, but it is yet to be shown whether this yields higher reproducibility or better sensitivity and specificity than devices without eye-tracking systems.

OCT Systems for Surgical Guidance

As described earlier in this review, OCT is already being used for surgical planning and follow-up. In addition, there has been progress in the development of intraoperative OCT systems. Intraoperative OCT was first demonstrated in anterior segment surgery, where a 1310-nm system was coupled to an operating microscope.[141] The use of a handheld OCT retinal imaging device has also been demonstrated for use in patients undergoing vitrectomy, after removing either the ILM or epiretinal membrane, to better visualize the macular disease.[142] It is possible that the development of an intraoperative approach may be further improved using a projection of a virtual OCT image over the surgical site and within the line of sight of the surgeon,[143] but the means of implementing this technique for surgery still has to be investigated.

Animal OCT Imaging

The noninvasive nature of image acquisition, together with the commercialization of systems optimized for laboratory use has resulted in a recent increase in the number of animal studies using OCT. Two- and three-dimensional scanning with OCT is appealing, because the same animals can be observed over time in vivo, making longitudinal studies of ocular structures possible without the need to kill animals at various time points and obtain histologic sections. Not only does this method reduce the number of animals needed for experiments, it is also superior to cross-sectional experiments that require different animals for different time points. The following briefly summarizes recent studies using OCT in animals, in small to large animal models.

The eyes of small animal models commonly used in developmental biology, such as xenopus laevis larvae[144] and zebrafish embryos[145] have successfully been imaged with OCT. Rodent imaging with OCT is becoming increasingly popular, given their relatively low cost and short lifespan and therefore shorter time for disease progression. In addition, many transgenic models are easy for researchers to access. OCT has been used to study ocular dimensions[146] and characterize normal eye growth[147] as well as growth of eyes in mouse models of myopia.[148] Mouse models of retinal degeneration have been imaged using TD-OCT,[149,150] and healthy and degenerative mice with SD-OCT.[151–158]

Recently, methods for automatically obtaining measurements from mouse OCT images have been presented.[159,160] Images taken in an anesthetized mouse, held in place using a stage with a glass coverslip to neutralize the strong refractive power of the mouse cornea were shown to be reproducible.[159] This indicates that 3D SD-OCT imaging of the mouse retina may be useful for longitudinal studies of retinal structure in mice.

Rats also provide an interesting platform for studying structural changes in the retina and optic nerve in response to injury or disease. Given their larger eyes, it is less complicated to focus on the retina than in the mouse. Retina and optic nerve imaging has been demonstrated in rat models of retinal degeneration,[151] retinal vein occlusion,[161] retinal ganglion cell degeneration post nerve-crush injury[162,163] and elevated intraocular pressure,[164] suggesting that there is also potential for rats to be used for longitudinal studies with OCT.

The eyes of larger animal models, such as chickens with retinal degeneration,[165] have been imaged. Researchers have also used OCT to examine birds of prey,[166] pigs,[167,168] cats,[169] and rabbits.[170–178] These animals have eyes that are comparable in size to the human eye, which means large modifications of the OCT system optics are not necessary.

Nonhuman primate models are especially appealing for studies with OCT, since their ocular size and structure closely match those of the human eye. Nonhuman primate imaging may provide novel insight into the mechanical damage to the RNFL and ONH associated with increased IOP, as is often seen in glaucoma. PS-OCT has been used to look at the birefringence of the RNFL,[129,179,180] and RNFL thickness was measured in eyes with unilateral, laser-induced ocular hypertension.[181,182] Strouthidis et al.[183] examined 3D SD-OCT images of the optic nerve in nonhuman primate eyes. They visualized the termina-

tion of Bruch's membrane, border tissue, and the anterior scleral canal opening and showed that these structures correlated to disc photos[184] and histology.[185] This set the stage for a study of alterations in the ONH that are due to increased intraocular pressure.[186]

Ultimately, longitudinal OCT studies of small and large animals may help evaluate the efficacy of pharmacologic agents, stem cell therapies, surgical intervention, and retinal prosthetics while reducing the required number of animals. OCT has the potential to provide a better understanding of disease development and progression in transgenic and other models of disease, which may eventually translate to improved clinical assessment and understanding of disease.

Conclusion

The use of OCT imaging in ophthalmology has increased steadily in recent years, in part due to technological improvements such as scanning speed, sensitivity and resolution. The field continues to grow and transform the way glaucoma and retinal diseases are monitored. With 3D imaging, there are new ways to visualize pathologic features and corresponding challenges to overcome. Current approaches, such as RNFL thickness maps and C-mode visualization, attempt to summarize structural information. These methods are not necessarily optimized for efficient cross-sectional and longitudinal analysis, but with technological improvements such as longer wavelength imaging, SS-OCT, AO-OCT, and PS-OCT on the horizon, even more structural detail will be available. Translating these techniques to the clinic has already begun and many could eventually be made available to the clinician. A combined slit-lamp/OCT system that allows the clinician to access structural information during a routine examination may eventually be available, as may a portable operating room system. The use of OCT in animal models has the potential to further understanding of disease while offering a platform for testing novel approaches to treatment, as well as for innovations of the OCT technique itself. The future of OCT is promising, but with some constraints that, if history is any indication, will become the basis for future advancement.

References

1. Fercher AF, Mengedoht K, Werner W. Eye-length measurement by interferometry with partially coherent light. *Opt Lett.* 1988; 13:186–188.
2. Huang D, Swanson EA, Lin CP, et al. Optical coherence tomography. *Science.* 1991;254:1178–1181.
3. Fercher AF, Hitzenberger CK, Drexler W, Kamp G, Sattmann H. In vivo optical coherence tomography. *Am J Ophthalmol.* 1993; 116:113–114.
4. Puliafito CA, Hee MR, Lin CP, et al. Imaging of macular diseases with optical coherence tomography. *Ophthalmology.* 1995;102: 217–229.
5. Hee MR, Izatt JA, Swanson EA, et al. Optical coherence tomography of the human retina. *Arch Ophthalmol.* 1995;113:325–332.
6. Izatt JA, Hee MR, Swanson EA, et al. Micrometer-scale resolution imaging of the anterior eye in vivo with optical coherence tomography. *Arch Ophthalmol.* 1994;112:1584–1589.
7. Swanson EA, Izatt JA, Hee MR, et al. In vivo retinal imaging by optical coherence tomography. *Opt Lett.* 1993;18:1864–1866.
8. Schuman JS, Hee MR, Arya AV, et al. Optical coherence tomography: a new tool for glaucoma diagnosis. *Curr Opin Ophthalmol.* 1995;6:89–95.
9. Schuman JS, Hee MR, Puliafito CA, et al. Quantification of nerve fiber layer thickness in normal and glaucomatous eyes using optical coherence tomography. *Arch Ophthalmol.* 1995;113: 586–596.
10. Schuman JS, Pedut-Kloizman T, Hertzmark E, et al. Reproducibility of nerve fiber layer thickness measurements using optical coherence tomography. *Ophthalmology.* 1996;103:1889–1898.
11. Drexler W, Morgner U, Kartner FX, et al. In vivo ultrahigh-resolution optical coherence tomography. *Opt Lett.* 1999;24: 1221–1223.
12. Lim H, Jiang Y, Wang Y, Huang YC, Chen Z, Wise FW. Ultrahigh-resolution optical coherence tomography with a fiber laser source at 1 microm. *Opt Lett.* 2005;30:1171–1173.
13. Unterhuber A, Povazay B, Bizheva K, et al. Advances in broad bandwidth light sources for ultrahigh resolution optical coherence tomography. *Phys Med Biol.* 2004;49:1235–1246.
14. Wojtkowski M, Leitgeb R, Kowalczyk A, Bajraszewski T, Fercher A. In vivo human retinal imaging by Fourier-domain optical coherence tomography. *J Biomed Opt.* 2002;7:457–463.
15. Fercher A, Hitzenberger C, Kamp G, Elzaiat S. Measurement of intraocular distances by backscattering spectral interferometry. *Opt Commun.* 1995;117:43–48.
16. Choma MA, Hsu K, Izatt JA. Swept source optical coherence tomography using an all-fiber 1300-nm ring laser source. *J Biomed Opt.* 2005;10:44009.
17. de Boer JF, Cense B, Park BH, Pierce MC, Tearney GJ, Bouma BE. Improved signal-to-noise ratio in spectral-domain compared with time-domain optical coherence tomography. *Opt Lett.* 2003;28: 2067–2069.
18. Leitgeb R, Wojtkowski M, Kowalczyk A, Hitzenberger CK, Sticker M, Fercher AF. Spectral measurement of absorption by spectroscopic frequency-domain optical coherence tomography. *Opt Lett.* 2000;25:820–822.
19. Nassif N, Cense B, Park BH, et al. In vivo human retinal imaging by ultrahigh-speed spectral domain optical coherence tomography. *Opt Lett.* 2004;29:480–482.
20. Wojtkowski M, Srinivasan V, Fujimoto JG, et al. Three-dimensional retinal imaging with high-speed ultrahigh-resolution optical coherence tomography. *Ophthalmology.* 2005;112:1734–1746.
21. Zhang J, Rao B, Chen Z. Swept source based fourier domain functional optical coherence tomography. *Conf Proc IEEE Eng Med Biol Soc.* 2005;7:7230–7233.
22. Yun SH, Tearney G, de Boer J, Bouma B. Pulsed-source and swept-source spectral-domain optical coherence tomography with reduced motion artifacts. *Opt Express.* 2004;12:5614–5624.
23. Choma M, Sarunic M, Yang C, Izatt J. Sensitivity advantage of swept source and Fourier domain optical coherence tomography. *Opt Express.* 2003;11:2183–2189.
24. Drexler W, Morgner U, Ghanta RK, Kartner FX, Schuman JS, Fujimoto JG. Ultrahigh-resolution ophthalmic optical coherence tomography. *Nat Med.* 2001;7:502–507.
25. Leitgeb R, Hitzenberger C, Fercher A. Performance of fourier domain vs. time domain optical coherence tomography. *Opt Express.* 2003;11:889–894.
26. Potsaid B, Gorczynska I, Srinivasan VJ, et al. Ultrahigh speed spectral / Fourier domain OCT ophthalmic imaging at 70,000 to 312,500 axial scans per second. *Opt Express.* 2008;16:15149–15169.
27. Srinivasan VJ, Adler DC, Chen Y, et al. Ultrahigh-speed optical coherence tomography for three-dimensional and en face imaging of the retina and optic nerve head. *Invest Ophthalmol Vis Sci.* 2008;49:5103–5110.
28. Bowd C, Weinreb RN, Williams JM, Zangwill LM. The retinal nerve fiber layer thickness in ocular hypertensive, normal, and glaucomatous eyes with optical coherence tomography. *Arch Ophthalmol.* 2000;118:22–26.
29. Bowd C, Zangwill LM, Berry CC, et al. Detecting early glaucoma by assessment of retinal nerve fiber layer thickness and visual function. *Invest Ophthalmol Vis Sci.* 2001;42:1993–2003.
30. Hoh ST, Greenfield DS, Mistlberger A, Liebmann JM, Ishikawa H, Ritch R. Optical coherence tomography and scanning laser polarimetry in normal, ocular hypertensive, and glaucomatous eyes. *Am J Ophthalmol.* 2000;129:129–135.
31. Mistlberger A, Liebmann JM, Greenfield DS, et al. Heidelberg retina tomography and optical coherence tomography in normal,

ocular-hypertensive, and glaucomatous eyes. *Ophthalmology.* 1999;106:2027–2032.
32. Pieroth L, Schuman JS, Hertzmark E, et al. Evaluation of focal defects of the nerve fiber layer using optical coherence tomography. *Ophthalmology.* 1999;106:570–579.
33. Zangwill LM, Williams J, Berry CC, Knauer S, Weinreb RN. A comparison of optical coherence tomography and retinal nerve fiber layer photography for detection of nerve fiber layer damage in glaucoma. *Ophthalmology.* 2000;107:1309–1315.
34. Wollstein G, Ishikawa H, Wang J, Beaton SA, Schuman JS. Comparison of three optical coherence tomography scanning areas for detection of glaucomatous damage. *Am J Ophthalmol.* 2005; 139:39–43.
35. Schuman JS. Spectral domain optical coherence tomography for glaucoma (an AOS thesis). *Trans Am Ophthalmol Soc.* 2008;106: 426–458.
36. Kim JS, Ishikawa H, Sung KR, et al. Retinal nerve fibre layer thickness measurement reproducibility improved with spectral domain optical coherence tomography. *Br J Ophthalmol.* 2009; 93:1057–1063.
37. Gabriele ML, Ishikawa H, Wollstein G, et al. Peripapillary nerve fiber layer thickness profile determined with high speed, ultrahigh resolution optical coherence tomography high-density scanning. *Invest Ophthalmol Vis Sci.* 2007;48:3154–3160.
38. Ishikawa H, Stein DM, Wollstein G, Beaton S, Fujimoto JG, Schuman JS. Macular segmentation with optical coherence tomography. *Invest Ophthalmol Vis Sci.* 2005;46:2012–2017.
39. Kim JS, Ishikawa H, Gabriele ML, et al. Retinal nerve fiber layer thickness measurement comparability between time domain optical coherence tomography (OCT) and spectral domain OCT. *Invest Ophthalmol Vis Sci.* 2010;51:896–902.
40. Jorgensen TM, Thomadsen J, Christensen U, Soliman W, Sander B. Enhancing the signal-to-noise ratio in ophthalmic optical coherence tomography by image registration–method and clinical examples. *J Biomed Opt.* 2007;12:041208.
41. Ramrath L, Moreno G, Mueller H, Bonin T, Huettmann G, Schweikard A. Towards multi-directional OCT for speckle noise reduction. *Med Image Comput Comput Assist Interv Int Conf Med Image Comput Comput Assist Interv.* 2008;11:815–823.
42. Ricco S, Chen M, Ishikawa H, Wollstein G, Schuman JS. Correcting motion artifacts in retinal spectral domain optical coherence tomography via image registration. *Med Image Comput Comput Assist Interv Proceed.* 2009;5761:100–107.
43. Xu J, Ishikawa H, Wollstein G, Schuman JS. Retinal vessel segmentation on SLO image. *Conf Proc IEEE Eng Med Biol Soc.* 2008;2008:2258–2261.
44. Ferguson RD, Hammer DX, Paunescu LA, Beaton S, Schuman JS. Tracking optical coherence tomography. *Opt Lett.* 2004;29: 2139–2141.
45. Hammer DX, Ferguson RD, Magill JC, et al. Active retinal tracker for clinical optical coherence tomography systems. *J Biomed Opt.* 2005;10:024038.
46. Ishikawa H, Gabriele ML, Wollstein G, et al. Retinal nerve fiber layer assessment using optical coherence tomography with active optic nerve head tracking. *Invest Ophthalmol Vis Sci.* 2006;47: 964–967.
47. Cense B, Chen TC, Park BH, Pierce MC, de Boer JF. In vivo birefringence and thickness measurements of the human retinal nerve fiber layer using polarization-sensitive optical coherence tomography. *J Biomed Opt.* 2004;9:121–125.
48. Cense B, Chen TC, Park BH, Pierce MC, de Boer JF. Thickness and birefringence of healthy retinal nerve fiber layer tissue measured with polarization-sensitive optical coherence tomography. *Invest Ophthalmol Vis Sci.* 2004;45:2606–2612.
49. Yamanari M, Miura M, Makita S, Yatagai T, Yasuno Y. Phase retardation measurement of retinal nerve fiber layer by polarization-sensitive spectral-domain optical coherence tomography and scanning laser polarimetry. *J Biomed Opt.* 2008;13:014013.
50. Gupta V, Gupta P, Singh R, Dogra MR, Gupta A. Spectral-domain Cirrus high-definition optical coherence tomography is better than time-domain Stratus optical coherence tomography for evaluation of macular pathologic features in uveitis. *Am J Ophthalmol.* 2008;145:1018–1022.
51. Koizumi H, Spaide RF, Fisher YL, Freund KB, Klancnik JM Jr, Yannuzzi LA. Three-dimensional evaluation of vitreomacular traction and epiretinal membrane using spectral-domain optical coherence tomography. *Am J Ophthalmol.* 2008;145:509–517.
52. Mojana F, Cheng L, Bartsch DU, et al. The role of abnormal vitreomacular adhesion in age-related macular degeneration: spectral optical coherence tomography and surgical results. *Am J Ophthalmol.* 2008;146:218–227.
53. Punjabi OS, Flynn HW Jr, Knighton RW, et al. Spectral domain optical coherence tomography for proliferative diabetic retinopathy with subhyaloid hemorrhage. *Ophthalmic Surg Lasers Imaging.* 2008;39:494–496.
54. Schmidt-Erfurth U, Leitgeb RA, Michels S, et al. Three-dimensional ultrahigh-resolution optical coherence tomography of macular diseases. *Invest Ophthalmol Vis Sci.* 2005;46:3393–3402.
55. Srinivasan VJ, Wojtkowski M, Witkin AJ, et al. High-definition and 3-dimensional imaging of macular pathologies with high-speed ultrahigh-resolution optical coherence tomography. *Ophthalmology.* 2006;113:2054 e2051–2014.
56. Oh J, Smiddy WE, Flynn HW Jr, Gregori G, Lujan B. Photoreceptor inner/outer segment defect imaging by spectral domain OCT and visual prognosis after macular hole surgery. *Invest Ophthalmol Vis Sci.* 2010;51:1651–1658.
57. Sano M, Shimoda Y, Hashimoto H, Kishi S. Restored photoreceptor outer segment and visual recovery after macular hole closure. *Am J Ophthalmol.* 2009;147:313–318 e311.
58. Inoue M, Watanabe Y, Arakawa A, Sato S, Kobayashi S, Kadonosono K. Spectral-domain optical coherence tomography images of inner/outer segment junctions and macular hole surgery outcomes. *Graefes Arch Clin Exp Ophthalmol.* 2009;247:325–330.
59. Chung EJ, Lew YJ, Lee H, Koh HJ. OCT-guided hyaloid release for vitreomacular traction syndrome. *Korean J Ophthalmol.* 2008; 22:169–173.
60. Falkner-Radler CI, Glittenberg C, Binder S. Spectral domain high-definition optical coherence tomography in patients undergoing epiretinal membrane surgery. *Ophthalmic Surg Lasers Imaging.* 2009;40:270–276.
61. Michalewska Z, Michalewski J, Cisiecki S, Adelman R, Nawrocki J. Correlation between foveal structure and visual outcome following macular hole surgery: a spectral optical coherence tomography study. *Graefes Arch Clin Exp Ophthalmol.* 2008;246:823–830.
62. Uchino E, Uemura A, Doi N, Ohba N. Postsurgical evaluation of idiopathic vitreomacular traction syndrome by optical coherence tomography. *Am J Ophthalmol.* 2001;132:122–123.
63. Chang LK, Fine HF, Spaide RF, Koizumi H, Grossniklaus HE. Ultrastructural correlation of spectral-domain optical coherence tomographic findings in vitreomacular traction syndrome. *Am J Ophthalmol.* 2008;146:121–127.
64. Sayegh RG, Georgopoulos M, Geitzenauer W, Simader C, Kiss C, Schmidt-Erfurth U. High-resolution optical coherence tomography after surgery for vitreomacular traction: a 2-year follow-up. *Ophthalmology.* 2010;117:2010–2017-e1–2.
65. Freeman SR, Kozak I, Cheng L, et al. Optical coherence tomography-raster scanning and manual segmentation in determining drusen volume in age-related macular degeneration. *Retina.* 2010;30:431–435.
66. Yi K, Mujat M, Park BH, et al. Spectral domain optical coherence tomography for quantitative evaluation of drusen and associated structural changes in non-neovascular age-related macular degeneration. *Br J Ophthalmol.* 2009;93:176–181.
67. Cabrera DeBuc D, Somfai GM. Early detection of retinal thickness changes in diabetes using optical coherence tomography. *Med Sci Monit.* 2010;16:MT15–MT21.
68. van Dijk HW, Kok PH, Garvin M, et al. Selective loss of inner retinal layer thickness in type 1 diabetic patients with minimal diabetic retinopathy. *Invest Ophthalmol Vis Sci.* 2009;50:3404–3409.
69. Huang J, Liu X, Wu Z, et al. Macular and retinal nerve fiber layer thickness measurements in normal eyes with the Stratus OCT, the Cirrus HD-OCT, and the Topcon 3D OCT-1000. *J Glaucoma.* 2011;20:118–125.

70. Koleva-Georgieva D, Sivkova N. Assessment of serous macular detachment in eyes with diabetic macular edema by use of spectral-domain optical coherence tomography. *Graefes Arch Clin Exp Ophthalmol.* 2009;247:1461–1469.
71. Arichika S, Hangai M, Yoshimura N. Correlation between thickening of the inner and outer retina and visual acuity in patients with epiretinal membrane. *Retina.* 2010;30:503–508.
72. Nunes S, Pereira I, Santos A, Bernardes R, Cunha-Vaz J. Central retinal thickness measured with HD-OCT shows a weak correlation with visual acuity in eyes with CSME. *Br J Ophthalmol.* 2010;94:1201–1204.
73. Patel PJ, Chen FK, da Cruz L, Tufail A. Segmentation error in Stratus optical coherence tomography for neovascular age-related macular degeneration. *Invest Ophthalmol Vis Sci.* 2009;50:399–404.
74. Sadda SR, Wu Z, Walsh AC, et al. Errors in retinal thickness measurements obtained by optical coherence tomography. *Ophthalmology.* 2006;113:285–293.
75. Keane PA, Mand PS, Liakopoulos S, Walsh AC, Sadda SR. Accuracy of retinal thickness measurements obtained with Cirrus optical coherence tomography. *Br J Ophthalmol.* 2009;93:1461–1467.
76. Giani A, Cigada M, Esmaili DD, et al. Artifacts in automatic retinal segmentation using different optical coherence tomography instruments. *Retina.* 2010;30:607–616.
77. Ishikawa H, Kim J, Friberg TR, et al. Three-dimensional optical coherence tomography (3D-OCT) image enhancement with segmentation-free contour modeling C-mode. *Invest Ophthalmol Vis Sci.* 2009;50:1344–1349.
78. Alam S, Zawadzki RJ, Choi S, et al. Clinical application of rapid serial fourier-domain optical coherence tomography for macular imaging. *Ophthalmology.* 2006;113:1425–1431.
79. Cucu RG, Podoleanu AG, Rogers JA, Pedro J, Rosen RB. Combined confocal/en face T-scan-based ultrahigh-resolution optical coherence tomography in vivo retinal imaging. *Opt Lett.* 2006;31:1684–1686.
80. Spaide RF, Koizumi H, Pozzoni MC. Enhanced depth imaging spectral-domain optical coherence tomography. *Am J Ophthalmol.* 2008;146:496–500.
81. Lee EC, de Boer JF, Mujat M, Lim H, Yun SH. In vivo optical frequency domain imaging of human retina and choroid. *Opt Express.* 2006;14:4403–4411.
82. Miller DT, Qu J, Jonnal RS, Thorn K. Coherence gating and adaptive optics in the eye. In: Tuchin VV, Izatt JA, Fujimoto JG, eds. Coherence Domain Methods and Optical Coherence Tomography in Biomedicine VII. *Proc SPIE.* 2003;4596:65–72.
83. Zawadzki RJ, Jones SM, Olivier SS, et al. Adaptive-optics optical coherence tomography for high-resolution and high-speed 3D retinal in vivo imaging. *Opt Express.* 2005;13:8532–8546.
84. Zawadzki RJ, Choi SS, Jones SM, Oliver SS, Werner JS. Adaptive optics-optical coherence tomography: optimizing visualization of microscopic retinal structures in three dimensions. *J Opt Soc Am A Opt Image Sci Vis.* 2007;24:1373–1383.
85. Nolan W. Anterior segment imaging: ultrasound biomicroscopy and anterior segment optical coherence tomography. *Curr Opin Ophthalmol.* 2008;19:115–121.
86. Radhakrishnan S, Rollins AM, Roth JE, et al. Real-time optical coherence tomography of the anterior segment at 1310 nm. *Arch Ophthalmol.* 2001;119:1179–1185.
87. Huang D, Li Y, Radhakrishnan S. Optical coherence tomography of the anterior segment of the eye. *Ophthalmol Clin North Am.* 2004;17:1–6.
88. Kagemann L, Wollstein G, Ishikawa H, et al. Identification and assessment of Schlemm's canal by spectral-domain optical coherence tomography. *Invest Ophthalmol Vis Sci.* 2010;51:4054–4059.
89. Radhakrishnan S, Huang D, Smith SD. Optical coherence tomography imaging of the anterior chamber angle. *Ophthalmol Clin North Am.* 2005;18:375–381, vi.
90. Tang M, Li Y, Avila M, Huang D. Measuring total corneal power before and after laser in situ keratomileusis with high-speed optical coherence tomography. *J Cataract Refract Surg.* 2006;32:1843–1850.
91. Li Y, Shekhar R, Huang D. Corneal pachymetry mapping with high-speed optical coherence tomography. *Ophthalmology.* 2006;113:792–799 e792.
92. Li Y, Tang M, Zhang X, Salaroli CH, Ramos JL, Huang D. Pachymetric mapping with Fourier-domain optical coherence tomography. *J Cataract Refract Surg.* 2010;36:826–831.
93. Li Y, Netto MV, Shekhar R, Krueger RR, Huang D. A longitudinal study of LASIK flap and stromal thickness with high-speed optical coherence tomography. *Ophthalmology.* 2007;114:1124–1132.
94. Li Y, Meisler DM, Tang M, et al. Keratoconus diagnosis with optical coherence tomography pachymetry mapping. *Ophthalmology.* 2008;115:2159–2166.
95. Zeng Y, Liu Y, Liu X, et al. Comparison of lens thickness measurements using the anterior segment optical coherence tomography and A-scan ultrasonography. *Invest Ophthalmol Vis Sci.* 2009;50:290–294.
96. Christopoulos V, Kagemann L, Wollstein G, et al. In vivo corneal high-speed, ultra high-resolution optical coherence tomography. *Arch Ophthalmol.* 2007;125:1027–1035.
97. Yaqoob Z, Wu J, Yang C. Spectral domain optical coherence tomography: a better OCT imaging strategy. *BioTechniques.* 2005;39:S6–S13.
98. Lim H, Mujat M, Kerbage C, et al. High-speed imaging of human retina in vivo with swept-source optical coherence tomography. *Opt Express.* 2006;14:12902–12908.
99. Srinivasan VJ, Huber R, Gorczynska I, et al. High-speed, high-resolution optical coherence tomography retinal imaging with a frequency-swept laser at 850 nm. *Opt Lett.* 2007;32:361–363.
100. de Bruin DM, Burnes DL, Loewenstein J, et al. In vivo three-dimensional imaging of neovascular age-related macular degeneration using optical frequency domain imaging at 1050 nm. *Invest Ophthalmol Vis Sci.* 2008;49:4545–4552.
101. Yasuno Y, Hong Y, Makita S, et al. In vivo high-contrast imaging of deep posterior eye by 1-microm swept source optical coherence tomography and scattering optical coherence angiography. *Opt Express.* 2007;15:6121–6139.
102. Povazay B, Hermann B, Unterhuber A, et al. Three-dimensional optical coherence tomography at 1050 nm versus 800 nm in retinal pathologies: enhanced performance and choroidal penetration in cataract patients. *J Biomed Opt.* 2007;12:041211.
103. Yasuno Y, Miura M, Kawana K, et al. Visualization of sub-retinal pigment epithelium morphologies of exudative macular diseases by high-penetration optical coherence tomography. *Invest Ophthalmol Vis Sci.* 2009;50:405–413.
104. Yun S, Tearney G, de Boer J, Iftimia N, Bouma B. High-speed optical frequency-domain imaging. *Opt Express.* 2003;11:2953–2963.
105. Yasuno Y, Madjarova VD, Makita S, et al. Three-dimensional and high-speed swept-source optical coherence tomography for in vivo investigation of human anterior eye segments. *Opt Express.* 2005;13:10652–10664.
106. Miura M, Mori H, Watanabe Y, et al. Three-dimensional optical coherence tomography of granular corneal dystrophy. *Cornea.* 2007;26:373–374.
107. Asrani S, Sarunic M, Santiago C, Izatt J. Detailed visualization of the anterior segment using fourier-domain optical coherence tomography. *Arch Ophthalmol.* 2008;126:765–771.
108. Yasuno Y, Yamanari M, Kawana K, Oshika T, Miura M. Investigation of post-glaucoma-surgery structures by three-dimensional and polarization sensitive anterior eye segment optical coherence tomography. *Opt Express.* 2009;17:3980–3996.
109. Babcock HW. The possibility of compensating astronomical seeing. *Publ Astron Soc Pac.* 1953;65:229–236.
110. Hardy JW. Adaptive optics: a new technology for the control of light. *Proc IEEE.* 1978;66:651–697.
111. Liang J, Williams DR, Miller DT. Supernormal vision and high-resolution retinal imaging through adaptive optics. *J Opt Soc Am A Opt Image Sci Vis.* 1997;14:2884–2892.
112. Roorda A, Williams DR. The arrangement of the three cone classes in the living human eye. *Nature.* 1999;397:520–522.
113. Hermann B, Fernandez EJ, Unterhuber A, et al. Adaptive-optics ultrahigh-resolution optical coherence tomography. *Opt Lett.* 2004;29:2142–2144.

114. Donnelly WJ, 3rd, Roorda A. Optimal pupil size in the human eye for axial resolution. *J Opt Soc Am A Opt Image Sci Vis.* 2003;20: 2010–2015.
115. Artal P, Guirao A, Berrio E, Williams DR. Compensation of corneal aberrations by the internal optics in the human eye. *J Vis.* 2001; 1:1–8.
116. Fernandez E, Drexler W. Influence of ocular chromatic aberration and pupil size on transverse resolution in ophthalmic adaptive optics optical coherence tomography. *Opt Express.* 2005;13: 8184–8197.
117. Fernandez EJ, Unterhuber A, Povazay B, Hermann B, Artal P, Drexler W. Chromatic aberration correction of the human eye for retinal imaging in the near infrared. *Opt Express.* 2006;14:6213–6225.
118. Zhang Y, Rha J, Jonnal R, Miller D. Adaptive optics parallel spectral domain optical coherence tomography for imaging the living retina. *Opt Express.* 2005;13:4792–4811.
119. Zhang Y, Cense B, Rha J, et al. High-speed volumetric imaging of cone photoreceptors with adaptive optics spectral-domain optical coherence tomography. *Opt Express.* 2006;14:4380–4394.
120. Hammer DX, Iftimia NV, Ferguson RD, et al. Foveal fine structure in retinopathy of prematurity: an adaptive optics Fourier domain optical coherence tomography study. *Invest Ophthalmol Vis Sci.* 2008;49:2061–2070.
121. Choi SS, Zawadzki RJ, Keltner JL, Werner JS. Changes in cellular structures revealed by ultra-high resolution retinal imaging in optic neuropathies. *Invest Ophthalmol Vis Sci.* 2008;49:2103–2119.
122. Fernandez EJ, Povazay B, Hermann B, et al. Three-dimensional adaptive optics ultrahigh-resolution optical coherence tomography using a liquid crystal spatial light modulator. *Vision Res.* 2005;45:3432–3444.
123. Zawadzki RJ, Choi SS, Fuller AR, Evans JW, Hamann B, Werner JS. Cellular resolution volumetric in vivo retinal imaging with adaptive optics-optical coherence tomography. *Opt Express.* 2009;17: 4084–4094.
124. Burns SA, Tumbar R, Elsner AE, Ferguson D, Hammer DX. Large-field-of-view, modular, stabilized, adaptive-optics-based scanning laser ophthalmoscope. *J Opt Soc Am A Opt Image Sci Vis.* 2007; 24:1313–1326.
125. de Boer JF, Milner TE, van Gemert MJ, Nelson JS. Two-dimensional birefringence imaging in biological tissue by polarization-sensitive optical coherence tomography. *Opt Lett.* 1997;22:934–936.
126. Wang XJ, Milner TE, de Boer JF, Zhang Y, Pashley DH, Nelson JS. Characterization of dentin and enamel by use of optical coherence tomography. *Appl Opt.* 1999;38:2092–2096.
127. Saxer CE, de Boer JF, Park BH, Zhao Y, Chen Z, Nelson JS. High-speed fiber based polarization-sensitive optical coherence tomography of in vivo human skin. *Opt Lett.* 2000;25:1355–1357.
128. Drexler W, Stamper D, Jesser C, et al. Correlation of collagen organization with polarization sensitive imaging of in vitro cartilage: implications for osteoarthritis. *J Rheumatol.* 2001;28: 1311–1318.
129. Ducros MG, Marsack JD, Rylander HG 3rd, Thomsen SL, Milner TE. Primate retina imaging with polarization-sensitive optical coherence tomography. *J Opt Soc Am A Opt Image Sci Vis.* 2001; 18:2945–2956.
130. Yamanari M, Lim Y, Makita S, Yasuno Y. Visualization of phase retardation of deep posterior eye by polarization-sensitive swept-source optical coherence tomography with 1-microm probe. *Opt Express.* 2009;17:12385–12396.
131. Pircher M, Gotzinger E, Findl O, et al. Human macula investigated in vivo with polarization-sensitive optical coherence tomography. *Invest Ophthalmol Vis Sci.* 2006;47:5487–5494.
132. Gotzinger E, Pircher M, Geitzenauer W, et al. Retinal pigment epithelium segmentation by polarization sensitive optical coherence tomography. *Opt Express.* 2008;16:16410–16422.
133. Cense B, Gao W, Brown JM, et al. Retinal imaging with polarization-sensitive optical coherence tomography and adaptive optics. *Opt Express.* 2009;17:21634–21651.
134. Miura M, Yamanari M, Iwasaki T, et al. Imaging polarimetry in age-related macular degeneration. *Invest Ophthalmol Vis Sci.* 2008;49:2661–2667.
135. Ahlers C, Gotzinger E, Pircher M, et al. Imaging of the retinal pigment epithelium in age-related macular degeneration using polarization-sensitive optical coherence tomography. *Invest Ophthalmol Vis Sci.* 2010;51:2149–2157.
136. Gotzinger E, Pircher M, Sticker M, Fercher AF, Hitzenberger CK. Measurement and imaging of birefringent properties of the human cornea with phase-resolved, polarization-sensitive optical coherence tomography. *J Biomed Opt.* 2004;9:94–102.
137. Hitzenberger CK, Gotzinger E, Pircher M. Birefringence properties of the human cornea measured with polarization sensitive optical coherence tomography. *Bull Soc Belge Ophtalmol.* 2006; (302):153–168.
138. Pircher M, Gotzinger E, Baumann B, Hitzenberger CK. Corneal birefringence compensation for polarization sensitive optical coherence tomography of the human retina. *J Biomed Opt.* 2007; 12:041210.
139. Gotzinger E, Pircher M, Dejaco-Ruhswurm I, Kaminski S, Skorpik C, Hitzenberger CK. Imaging of birefringent properties of keratoconus corneas by polarization-sensitive optical coherence tomography. *Invest Ophthalmol Vis Sci.* 2007;48:3551–3558.
140. Menke MN, Dabov S, Knecht P, Sturm V. Reproducibility of retinal thickness measurements in healthy subjects using spectralis optical coherence tomography. *Am J Ophthalmol.* 2009; 147:467–472.
141. Geerling G, Muller M, Winter C, et al. Intraoperative 2-dimensional optical coherence tomography as a new tool for anterior segment surgery. *Arch Ophthalmol.* 2005;123:253–257.
142. Dayani PN, Maldonado R, Farsiu S, Toth CA. Intraoperative use of handheld spectral domain optical coherence tomography imaging in macular surgery. *Retina.* 2009;29:1457–1468.
143. Galeotti J, Sajjad A, Wang B, et al. The OCT penlight: In-situ image guidance for microsurgery. Medical Imaging 2010: Visualization, Image-Guided Prodecures, and Modeling. *SPIE Med Imaging.* 2010;7625:2.0–2.6.
144. Boppart SA, Brezinski ME, Bouma BE, Tearney GJ, Fujimoto JG. Investigation of developing embryonic morphology using optical coherence tomography. *Dev Biol.* 1996;177:54–63.
145. Kagemann L, Ishikawa H, Zou J, et al. Repeated, noninvasive, high resolution spectral domain optical coherence tomography imaging of zebrafish embryos. *Mol Vis.* 2008;14:2157–2170.
146. Zhou X, Xie J, Shen M, et al. Biometric measurement of the mouse eye using optical coherence tomography with focal plane advancement. *Vision Res.* 2008;48:1137–1143.
147. Zhou X, Shen M, Xie J, et al. The development of the refractive status and ocular growth in C57BL/6 mice. *Invest Ophthalmol Vis Sci.* 2008;49:5208–5214.
148. Zhou X, Huang Q, An J, et al. Genetic deletion of the adenosine A2A receptor confers postnatal development of relative myopia in mice. *Invest Ophthalmol Vis Sci.* 2010;51:4362–4370.
149. Horio N, Kachi S, Hori K, et al. Progressive change of optical coherence tomography scans in retinal degeneration slow mice. *Arch Ophthalmol.* 2001;119:1329–1332.
150. Li Q, Timmers AM, Hunter K, et al. Noninvasive imaging by optical coherence tomography to monitor retinal degeneration in the mouse. *Invest Ophthalmol Vis Sci.* 2001;42:2981–2989.
151. Srinivasan VJ, Ko TH, Wojtkowski M, et al. Noninvasive volumetric imaging and morphometry of the rodent retina with high-speed, ultrahigh-resolution optical coherence tomography. *Invest Ophthalmol Vis Sci.* 2006;47:5522–5528.
152. Kocaoglu OP, Uhlhorn SR, Hernandez E, et al. Simultaneous fundus imaging and optical coherence tomography of the mouse retina. *Invest Ophthalmol Vis Sci.* 2007;48:1283–1289.
153. Kim KH, Puoris'haag M, Maguluri GN, et al. Monitoring mouse retinal degeneration with high-resolution spectral-domain optical coherence tomography. *J Vis.* 2008;8:17 11–11.
154. Fingler J, Readhead C, Schwartz DM, Fraser SE. Phase-contrast OCT imaging of transverse flows in the mouse retina and choroid. *Invest Ophthalmol Vis Sci.* 2008;49:5055–5059.

155. Huber G, Beck SC, Grimm C, et al. Spectral domain optical coherence tomography in mouse models of retinal degeneration. *Invest Ophthalmol Vis Sci.* 2009;50:5888–5895.
156. Xu J, Molday LL, Molday RS, Sarunic MV. In vivo imaging of the mouse model of X-linked juvenile retinoschisis with fourier domain optical coherence tomography. *Invest Ophthalmol Vis Sci.* 2009;50:2989–2993.
157. Maeda A, Golczak M, Maeda T, Palczewski K. Limited roles of Rdh8, Rdh12, and Abca4 in all-trans-retinal clearance in mouse retina. *Invest Ophthalmol Vis Sci.* 2009;50:5435–5443.
158. Fischer MD, Huber G, Beck SC, et al. Noninvasive, in vivo assessment of mouse retinal structure using optical coherence tomography. *PLoS One.* 2009;4:e7507.
159. Gabriele ML, Ishikawa H, Schuman JS, et al. Reproducibility of spectral-domain optical coherence tomography total retinal thickness measurements in mice. *Invest Ophthalmol Vis Sci.* 2010;51:6519–6523.
160. Ruggeri M, Tsechpenakis G, Jiao S, et al. Retinal tumor imaging and volume quantification in mouse model using spectral-domain optical coherence tomography. *Opt Express.* 2009;17:4074–4083.
161. Doukas J, Mahesh S, Umeda N, et al. Topical administration of a multi-targeted kinase inhibitor suppresses choroidal neovascularization and retinal edema. *J Cell Physiol.* 2008;216:29–37.
162. Bai Y, Xu J, Brahimi F, Zhuo Y, Sarunic MV, Saragovi HU. An agonistic anti-TrkB mAb causes sustained TrkB activation, delays RGC death, and protects the retinal structure in optic nerve axotomy and in glaucoma. *Invest Ophthalmol Vis Sci.* 2010;51:4722–4731.
163. Nagata A, Higashide T, Ohkubo S, Takeda H, Sugiyama K. In vivo quantitative evaluation of the rat retinal nerve fiber layer with optical coherence tomography. *Invest Ophthalmol Vis Sci.* 2009;50:2809–2815.
164. Guo L, Tsatourian V, Luong V, et al. En face optical coherence tomography: a new method to analyse structural changes of the optic nerve head in rat glaucoma. *Br J Ophthalmol.* 2005;89:1210–1216.
165. Huang Y, Cideciyan AV, Papastergiou GI, et al. Relation of optical coherence tomography to microanatomy in normal and rd chickens. *Invest Ophthalmol Vis Sci.* 1998;39:2405–2416.
166. Ruggeri M, Major JC, McKeown C, Knighton RW, Puliafito CA, Jiao S. Retinal structure of birds of prey revealed by ultra-high resolution spectral-domain optical coherence tomography. *Invest Ophthalmol Vis Sci.* 2010;51:5789–5795.
167. Gloesmann M, Hermann B, Schubert C, Sattmann H, Ahnelt PK, Drexler W. Histologic correlation of pig retina radial stratification with ultrahigh-resolution optical coherence tomography. *Invest Ophthalmol Vis Sci.* 2003;44:1696–1703.
168. Gekeler F, Szurman P, Grisanti S, et al. Compound subretinal prostheses with extra-ocular parts designed for human trials: successful long-term implantation in pigs. *Graefes Arch Clin Exp Ophthalmol.* 2007;245:230–241.
169. Gekeler F, Gmeiner H, Volker M, et al. Assessment of the posterior segment of the cat eye by optical coherence tomography (OCT). *Vet Ophthalmol.* 2007;10:173–178.
170. Kim ET, Kim C, Lee SW, Seo JM, Chung H, Kim SJ. Feasibility of microelectrode array (MEA) based on silicone-polyimide hybrid for retina prosthesis. *Invest Ophthalmol Vis Sci.* 2009;50:4337–4341.
171. Cong L, Sun D, Zhang Z, Jiao W, Rizzolo LJ, Peng S. A novel rabbit model for studying RPE transplantation. *Invest Ophthalmol Vis Sci.* 2008;49:4115–4125.
172. Ameri H, Kim JG, Ratanapakorn T, Chader GJ, Humayun MS. Intravitreal and subretinal injection of tissue plasminogen activator (tPA) in the treatment of experimentally created retinal vein occlusion in rabbits. *Retina.* 2008;28:350–355.
173. Ameri H, Chader GJ, Kim JG, Sadda SR, Rao NA, Humayun MS. The effects of intravitreous bevacizumab on retinal neovascular membrane and normal capillaries in rabbits. *Invest Ophthalmol Vis Sci.* 2007;48:5708–5715.
174. Qiu G, Stewart JM, Sadda S, et al. A new model of experimental subretinal neovascularization in the rabbit. *Exp Eye Res.* 2006;83:141–152.
175. Kozak I, Cheng L, Mendez T, Davidson MC, Freeman WR. Evaluation of the toxicity of subretinal triamcinolone acetonide in the rabbit. *Retina.* 2006;26:811–817.
176. Asejczyk-Widlicka M, Schachar RA, Pierscionek BK. Optical coherence tomography measurements of the fresh porcine eye and response of the outer coats of the eye to volume increase. *J Biomed Opt.* 2008;13:024002.
177. Reiser BJ, Ignacio TS, Wang Y, et al. In vitro measurement of rabbit corneal epithelial thickness using ultrahigh resolution optical coherence tomography. *Vet Ophthalmol.* 2005;8:85–88.
178. Hosseini K, Kholodnykh AI, Petrova IY, Esenaliev RO, Hendrikse F, Motamedi M. Monitoring of rabbit cornea response to dehydration stress by optical coherence tomography. *Invest Ophthalmol Vis Sci.* 2004;45:2555–2562.
179. Kemp NJ, Park J, Zaatari HN, Rylander HG, Milner TE. High-sensitivity determination of birefringence in turbid media with enhanced polarization-sensitive optical coherence tomography. *J Opt Soc Am A Opt Image Sci Vis.* 2005;22:552–560.
180. Rylander HG 3rd, Kemp NJ, Park J, Zaatari HN, Milner TE. Birefringence of the primate retinal nerve fiber layer. *Exp Eye Res.* 2005;81:81–89.
181. Harwerth RS, Vilupuru AS, Rangaswamy NV, Smith EL 3rd. The relationship between nerve fiber layer and perimetry measurements. *Invest Ophthalmol Vis Sci.* 2007;48:763–773.
182. Schuman JS, Pedut-Kloizman T, Pakter H, et al. Optical coherence tomography and histologic measurements of nerve fiber layer thickness in normal and glaucomatous monkey eyes. *Invest Ophthalmol Vis Sci.* 2007;48:3645–3654.
183. Strouthidis NG, Yang H, Fortune B, Downs JC, Burgoyne CF. Detection of optic nerve head neural canal opening within histomorphometric and spectral domain optical coherence tomography data sets. *Invest Ophthalmol Vis Sci.* 2009;50:214–223.
184. Strouthidis NG, Yang H, Reynaud JF, et al. Comparison of clinical and spectral domain optical coherence tomography optic disc margin anatomy. *Invest Ophthalmol Vis Sci.* 2009;50:4709–4718.
185. Strouthidis NG, Grimm J, Williams GA, Cull GA, Wilson DJ, Burgoyne CF. A comparison of optic nerve head morphology viewed by spectral domain optical coherence tomography and by serial histology. *Invest Ophthalmol Vis Sci.* 2010;51:1464–1474.
186. Fortune B, Yang H, Strouthidis NG, et al. The effect of acute intraocular pressure elevation on peripapillary retinal thickness, retinal nerve fiber layer thickness, and retardance. *Invest Ophthalmol Vis Sci.* 2009;50:4719–4726.